

**ARTICLE TYPE****A novel “spectral-ratio model fitting” to resolve complicated AGN X-ray spectral variations**Takuya Midooka\*<sup>1,2</sup> | Misaki Mizumoto<sup>3,4</sup> | Ken Ebisawa<sup>1,2</sup><sup>1</sup>Institute of Space and Astronautical Science (ISAS), Japan Aerospace Exploration Agency (JAXA), Kanagawa, Japan<sup>2</sup>Department of Astronomy, Graduate School of Science, The University of Tokyo, Tokyo, Japan<sup>3</sup>Hakubi Center, Kyoto University, Kyoto, Japan<sup>4</sup>Department of Astronomy, Graduate School of Science, Kyoto University, Kyoto, Japan**Correspondence**

\* Email: midooka@ac.jaxa.jp

Contemporary radiation-magnetohydrodynamic simulation of the AGNs predicts presence of the hot and strong accretion disk wind, which gets unstable far from the central region and turns into gas clumps. These inner-wind and outer clumps may be actually observed as the ultrafast outflows (UFOs) and the clumpy absorbers, respectively. We may call this picture as the “hot inner and clumpy outer wind model”. Observationally, it is challenging to place constraints on the origin of the UFOs and clumpy absorbers due to complicated spectral variations. We developed a novel method, “spectral-ratio model fitting”, to resolve parameter degeneracy of the clumpy absorbers and other spectral components. In this method, the parameters of the absorber in the line of sight are estimated from the ratio of the partially absorbed spectrum to the non-absorbed one. We applied this method to the narrow-line Seyfert 1 galaxy IRAS 13224–3809 observed by *XMM-Newton* in 2016 for 1.5 Ms, where the source showed extreme spectral variability and complex absorption features. As a result, we found that the soft spectral variation is mostly explained by a change of the covering fraction of the mildly-ionized clumpy absorbers, and that these absorbers are outflowing with such a high velocity that is comparable to that of the UFO ( $\sim 0.2$ – $0.3$  c). This result implies that the formation of the clumpy absorbers and the UFO shares the same origin, supporting the “hot inner and clumpy outer wind model”.

**KEYWORDS:**

methods: data analysis, accretion, accretion disks, galaxies: nuclei, X-rays: individual: IRAS 13224–3809

**1 | INTRODUCTION**

Active galactic nuclei (AGNs) are powered by accretion onto supermassive black holes (SMBHs). Recent observational and theoretical studies suggest that most AGN have multiple absorbers. Broadly speaking, three types of absorbers have been recognized. The first one is the *warm absorbers* (WAs). WAs are detected as absorption lines and edges in the soft X-ray band of  $\sim 65\%$  of nearby AGNs, especially in the radio-quiet Seyfert 1 galaxies (e.g., McKernan, Yaqoob, & Reynolds, 2007, Laha, Guainazzi, Dewangan, Chakravorty, & Kembhavi,

2014). These absorbers are known to be mildly ionized and blue-shifted with a velocity of  $\lesssim 2,000$  km/s.

The second one is the *ultrafast outflow* (UFO). Seyfert galaxies often have blue-shifted, highly ionized absorption lines in their 30–40 % X-ray energy spectra (Tombesi et al., 2010). The UFOs are thought to be outflowing winds from the accretion disk at very high velocities of 0.1–0.3 c. Since the UFOs have a larger solid angle than the relativistic jets (e.g., Nardini et al., 2015, Hagino et al., 2015), they can supply gas to a wider area of the host galaxy. UFO contribution to the co-evolution of the supermassive black holes (SMBHs) and the galaxies may be comparable to or even greater than that of the jets (e.g., A. R. King, 2010, A. King & Pounds, 2015).

The third one is the *partial covering absorbers*, which partially absorb the X-ray continuum in the line of sight. This is also called the “obscurer”, which causes simultaneous soft X-ray and UV absorption troughs in NGC 5548 (Kaastra et al., 2014).

IRAS 13224–3809 is a narrow-line Seyfert 1 (NLS1) galaxy with a SMBH of about  $10^{6-7} M_{\odot}$  ( $z=0.0658$ ). Using 1.5 Ms deep observations of IRAS 13224–3809 made by *XMM-Newton* in 2016, Parker et al. (2017) discovered UFO absorption lines. They claimed that the equivalent width of the UFO absorption lines and the X-ray luminosity are anti-correlated, while the line-of-sight velocity of the UFO is correlated with the luminosity. They argue that the disk wind is driven by the radiation pressure, so that the absorption lines were not detected when the wind was fully ionized due to intense X-ray radiations.

Two-dimensional radiation-magnetohydrodynamic (R-MHD) simulations of supercritical accretion flows show that the radiation pressure generates a disk wind, and that the wind becomes clumpy due to Rayleigh-Taylor instability at a large distance where the radiation pressure is dominant over the gravitational potential (Takeuchi, Ohsuga, & Mineshige, 2013). In addition to the Rayleigh-Taylor instability, contribution of the radiation hydrodynamic instability in the clump formation is suggested in three-dimensional R-MHD simulations (e.g., Kobayashi et al., 2018).

These inner-wind and outer clumps may be actually observed as the ultrafast outflows (UFOs) and the clumpy absorbers, respectively (“hot inner and clumpy outer wind model”; Mizumoto et al., 2019). The clumpy partial absorbers are represented by four observable parameters; partial covering fraction (CF), ionization parameter  $\xi$ , hydrogen column density  $N_{\text{H}}$ , and the line-of-sight velocity  $v_{\text{out}}$ . However, in the standard X-ray spectral analysis, parameters of the partial absorption by clumpy absorbers and other components such as WAs and soft-excess are often degenerate in the soft X-ray band.

In the present study, we adopt a new data analysis method which we may call “spectral-ratio model fitting” to the long campaign data of IRAS 13224–3809. The objective is to disentangle spectral parameter degeneracy amid the complex spectral variations, and to constrain parameters of the partial absorbers.

## 2 | OBSERVATIONS AND METHODS

### 2.1 | Observations and Data reduction

We used the 1.5 Ms data obtained by *XMM-Newton* EPIC-pn (Jansen et al., 2001, Strüder et al., 2001) in the summer of 2016 (Table 1 ). The EPIC-MOS data were not used because

**TABLE 1** Observation logs with *XMM-Newton* (pn)

Start Date	Obs ID	Net Exp. (s) <sup>a</sup>
2016 Jul 08	0780560101 <sup>b</sup>	53,333
2016 Jul 10	0780561301	122,231
2016 Jul 12	0780561401 <sup>b</sup>	113,522
2016 Jul 20	0780561501	119,582
2016 Jul 22	0780561601	118,232
2016 Jul 24	0780561701	117,300
2016 Jul 26	0792180101	122,702
2016 Jul 30	0792180201	119,916
2016 Aug 01	0792180301 <sup>b</sup>	108,568
2016 Aug 03	0792180401	108,038
2016 Aug 07	0792180501	111,833
2016 Aug 09	0792180601	115,994

<sup>a</sup> Sum of all the good time intervals.

<sup>b</sup> Unscheduled observations are included in these observation IDs. We combined the scheduled data and the unscheduled data.

its effective area is much smaller than that of the pn detector in the soft X-ray band. The pn data were reduced with SAS (version 19.1.0) to obtain the filtered event files. The unscheduled observations (See Table 1 ) were also used for the analysis to improve the statistics<sup>1</sup>. Good time intervals were calculated by removing the periods dominated by the flaring particle background when the PATTERN==0 count rate in 10–12 keV is larger than 0.4 counts s<sup>-1</sup>. We used circular regions of 250 physical unit (12.5'') radius and 1600 physical unit (75'') radius from the same CCD for extracting the source events and the background events, respectively. These region sizes are determined following to Chartas & Canas (2018) to maximize the signal-to-noise ratio. Also, the background region is carefully selected, avoiding chip edges and the region where the Cu background is high. Following the “SAS Data Analysis Threads”<sup>2</sup>, we extracted light curves, spectra, and responses in the 0.3–10.0 keV band applying the good time intervals and the source/background regions.

Since the X-ray spectral features (hardness ratio and absorption line depth etc.) are variable according to the luminosity, we created intensity-sliced spectra following Parker et al. (2017) and Pinto et al. (2018). First, all the 0.3–10.0 keV events from all the observation IDs are binned every 1 ks, and these time-bins are sorted in the order of the counts per bin. The total number of events being X, we defined 10 groups in order,

<sup>1</sup>In case of there were interruptions, for example, due to high radiation levels, the exposures taken after the interruptions are called unscheduled.

<sup>2</sup><https://www.cosmos.esa.int/web/xmm-newton/sas-thread-epic-filterbackground>  
<https://www.cosmos.esa.int/web/xmm-newton/sas-thread-pn-spectrum>  
<https://www.cosmos.esa.int/web/xmm-newton/sas-thread-rgs>

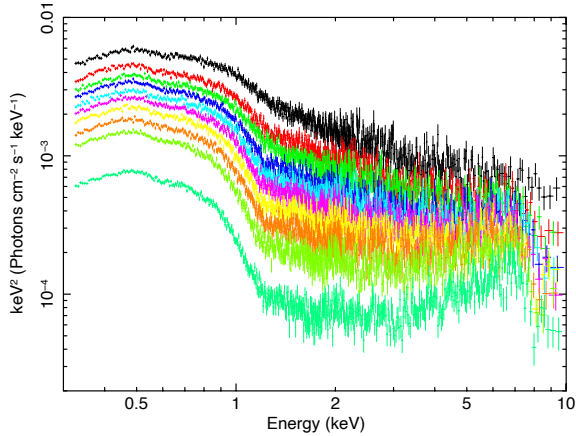


**FIGURE 1** The 10 intensity-sliced spectra obtained by *XMM-Newton* pn in 0.3–10.0 keV. The  $\nu F_\nu$  plot unfolded by the power-law with the index of 2 is shown.

**TABLE 2** Count rate threshold of intensity-sliced spectra (0.3–10.0 keV)

Division	Minimum (counts s <sup>-1</sup> )	Maximum (counts s <sup>-1</sup> )
A	7.55	12.51
B	6.09	7.55
C	5.21	6.09
D	4.46	5.21
E	3.92	4.46
F	3.34	3.92
G	2.74	3.34
H	2.23	2.74
I	1.63	2.23
J	0.29	1.63

so that each group has 0.1 X events in total. In this manner, 10 intensity-sliced spectra were created (Table 2). The sliced spectra were grouped with 8 and 16 spectral-bins in 0.3–2.0 keV and 2.0–10.0 keV, respectively. The intensity-sliced spectra are shown in Figure 1.

## 2.2 | Spectral components of IRAS 13224–3809 and the spectral-ratio analysis

The following depiction is adopted in the X-ray spectral model for this study. The continuum consists of the power-law (PL) and the soft-excess that contribute mainly above and below  $\sim 1$  keV, respectively. The spectral shape of the continuum does

not change significantly, while the continuum intensity and/or the PL index may vary.

The continuum is absorbed by several gases such as WA, UFO, and clumpy absorbers. UFOs are highly ionized and mainly absorb the hard X-rays above  $\sim 6$  keV. WAs do not change their geometry or ionization structure significantly in a timescale of a few weeks, while the partial covering fraction of the clumpy absorbers significantly changes on shorter timescales and significantly alters the spectral shape below  $\sim 5$  keV (e.g., Di Gesu et al., 2015, Midooka, Ebisawa, Mizumoto, & Sugawara, 2022).

Therefore, taking the spectral-ratio below 5 keV enables us to focus on the variability of the clumpy absorbers, canceling out the less time-variable spectral components. A significant merit of this method is that it is not necessary to determine the spectral shape of the continuum precisely.

## 2.3 | Method of the spectral-ratio analysis

Model spectral-ratios are created in the 0.3–5.0 keV band using XSPEC (version 12.12.0). Our aim is to extract the spectral change due to the clumpy absorber. Therefore, we consider a simple model spectrum (`powerlaw * zxcipcf`) in which the continuum `powerlaw` is covered by an ionized partial absorber. Since the response of any intensity-sliced spectra had only variations of less than 1%, model spectra are extracted using the response of the brightest spectrum A (see Table 2). A table model of the spectral-ratio is created by taking the ratio of the absorbed model spectra to the unabsorbed one with the same continuum parameters. This operation is repeated for the number of combinations of the parameter grids (Table 3).

Figure 2 shows examples of the model spectral-ratios when each of CF,  $N_{\text{H}}$ , and  $\xi$  is varied at several different values while the two other parameters are fixed (the velocity of the absorber is null). When the absorber is mildly ionized ( $\log \xi \sim 1.5$ – $3.0$ ), characteristic dip structures are seen in 0.8–1.0 keV. They are mainly created by Fe-L and Fe-M Unresolved Transition Array (UTA), and its depth, width, and shape are dependent on the ionization parameter and the column density. Ion population changes as the ionization increases, and the dip energy increases up to  $\sim 0.95$  keV. It is noteworthy that the dip energy never goes beyond  $\sim 1$  keV, no matter how much the gas is ionized. If observed spectral-ratios show dips at above 1 keV, that cannot be explained by the ionization, and strongly suggests that the clumpy absorber is blueshifted.

Now we see the observed ratio spectrum. The ratio of the fifth brightest spectrum (E) to the brightest spectrum (A) is shown in blue dots in Figure 3, where the dip structure is seen around 1.1–1.3 keV. We are going to compare the observed spectral-ratio with models, assuming that the spectrum A is unabsorbed (CF = 0). We consider an X-ray spectrum with

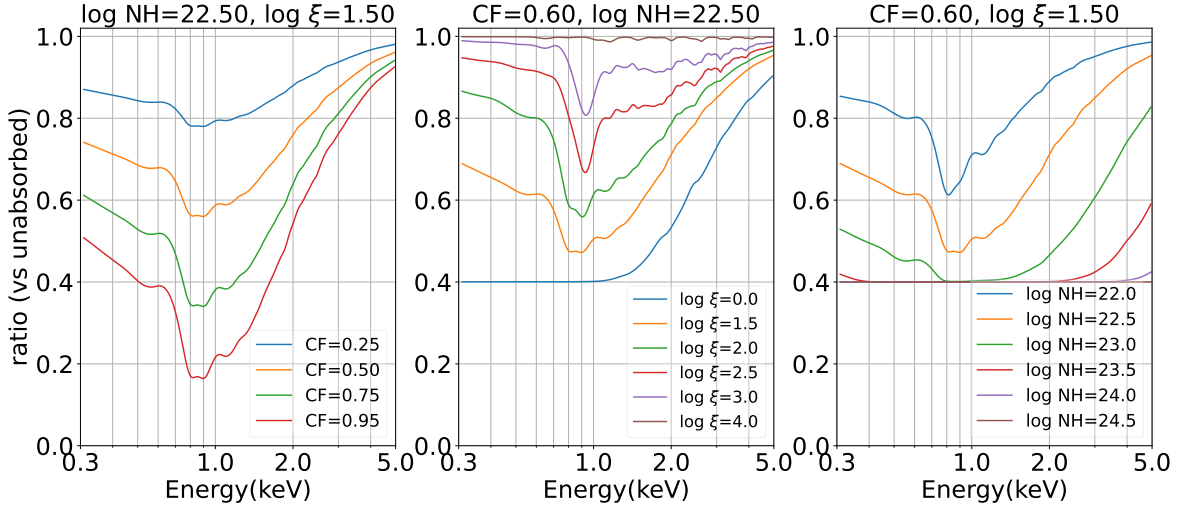


**FIGURE 2** Model spectral-ratios, where each of CF,  $N_{\text{H}}$ , and  $\xi$  (from left to right) is varied at several different values while the other two parameters are fixed. The absorber velocity is null.

CF = 0.5,  $\log N_{\text{H}} = 23.75$ ,  $\log \xi = 2.75$ , whose ratio to the unabsorbed spectrum is the orange curve in Figure 3. In this spectral-ratio model, the dip structure energy does not match with the observation (see Figure 2). Therefore, we introduce the absorber velocity ( $-0.25c$ ) to blue-shift the dip energy, and also the normalization is made 0.51 times (blue line in Figure 3). We see that the observed dip feature is explained well by the model spectral-ratio.

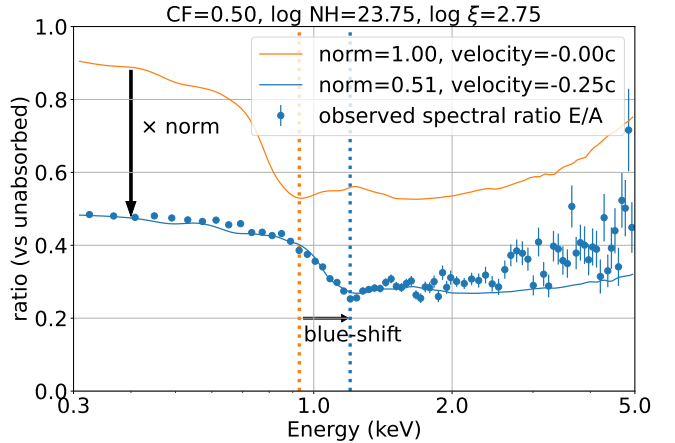
Variation of the model spectral-ratios when the velocity or the norm is varied is shown in Figure 4. The energy shift of the dip structure is apparent with the velocity variation, so the absorber velocity is expected to be constrained.

### 3 | DATA ANALYSIS AND RESULTS

#### 3.1 | Spectral-ratio fitting in the 0.3–5 keV band

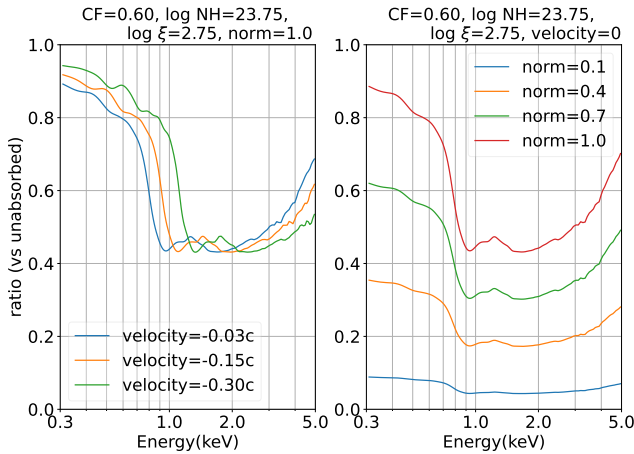
We made 9 spectral-ratios from the 10 observed intensity-sliced spectra. Model spectral-ratios were created using the parameter range in Table 3. Least-square fitting was performed for the 9 observed spectral-ratios, where models are linearly interpolated between the adjacent grid points.

Figure 5 shows examples of the spectral-ratio model fitting, where the lower panel shows residuals normalized by the statistical errors,  $(\text{data}-\text{model})/\text{error}$ . The free parameters are CF,  $\xi$ ,  $N_{\text{H}}$ ,  $v$ , and norm (which explains the level of the continuum flux). They are constrained well. While the  $N_{\text{H}}$  and  $\xi$  were not significantly variable, the other CF,  $v$ , and norm vary. The largest variation is seen in CF, where the partial covering fraction of the clumpy absorbers varies from 30%



**FIGURE 3** Blue dots show the observed spectral-ratio E/A. The orange line represents a model ratio between the absorbed and unabsorbed spectra, where the absorbed spectrum has CF = 0.5,  $\log N_{\text{H}} = 23.75$ , and  $\log \xi = 2.75$ . We find that the dip energy of the model spectral-ratio needs to be blue-shifted. After varying the norm and velocity, the orange line moves to the blue one, which fits to the observed ratio.

to 90%. This produces a characteristic soft X-ray band variation. The intrinsic flux also changes. The flux at the faintest spectrum is reduced to 30% of that at the brightest one. This indicates that the X-ray spectral variations result from a combination of intrinsic luminosity and partial absorber variations. It is noteworthy that the velocity of the partial absorber is very fast,  $\sim 0.3c$ , and that the velocity increases as the flux gets



**FIGURE 4** Model spectral-ratios, where the velocity (left) or the norm (right) of the absorbed spectrum is varied at several different values, while the other parameters are fixed.

**TABLE 3** Parameter ranges for the spectral-ratio model

Component	Minimum	Maximum
CF	0	1
velocity [c]	-0.3	0
$\log \xi$	0	3
$N_{\text{H}}$	$10^{22}$	$10^{25}$

brighter. This velocity is roughly consistent with that of the UFO. Therefore, it is inferred that clumpy absorbers and UFOs are produced by the same physical mechanisms.

For the fainter spectra at  $>2$  keV, the observed spectral-ratios tend to be higher than the models (middle and right panels in Figure 5), which is mainly due to the current assumption that the intrinsic spectral shape does not vary. If the spectra get “softer when brighter”, as is the case in many AGNs, these residuals could be explained. This topic will be closely investigated in our subsequent paper.

## 4 | CONCLUSION

A novel “spectral-ratio model fitting” was developed to resolve the degeneracy of the soft X-ray spectral components. Taking the spectral ratios of the intensity-sliced spectra below 5 keV makes the spectral variations due to partial absorbers conspicuous, by canceling out the less time-variable continuum and the warm absorber components. As a result, we succeeded in constraining the clump outflow velocity, which was comparable to that of the UFOs. We also found that these velocities get higher with increasing the X-ray luminosity.

## ACKNOWLEDGMENTS

This research has made use of data and software provided by the High Energy Astrophysics Science Archive Research Center (HEASARC), which is a service of the Astrophysics Science Division at NASA/GSFC and the High Energy Astrophysics Division of the Smithsonian Astrophysical Observatory. This study was based on observations obtained with *XMM-Newton*, ESA science missions with instruments and contributions directly funded by ESA Member States and NASA. This research was supported by JSPS Grant-in-Aid for JSPS Research Fellow Grant Number JP20J20809 (T.M.), JSPS KAKENHI Grant Number JP21K13958 (M.M). M.M. acknowledges support from the Hakubi project at Kyoto University.

## REFERENCES

- Chartas, G., & Canas, M. H. 2018, *The Astrophysical Journal*, 867, 103.
- Di Gesu, L., Costantini, E., Ebrero, J. et al. 2015, *Astronomy and Astrophysics*, 579, A42.
- Hagino, K., Odaka, H., Done, C., Gandhi, P., Watanabe, S., Sako, M., & Takahashi, T. 2015, *Monthly Notices of the Royal Astronomical Society*, 446, 663–676.
- Jansen, F., Lumb, D., Altieri, B. et al. 2001, *Astronomy & Astrophysics*, 365(1), L1-L6.
- Kaastra, J. S., Kriss, G. A., Cappi, M. et al. 2014, *Science*, 345, 64–68.
- King, A., & Pounds, K. 2015, *Annual Review of Astronomy and Astrophysics*, 53, 115–154.
- King, A. R. 2010, *Monthly Notices of the Royal Astronomical Society*, 402(3), 1516–1522.
- Kobayashi, H., Ohsuga, K., Takahashi, H. R., Kawashima, T., Asahina, Y., Takeuchi, S., & Mineshige, S. 2018, *Publications of the Astronomical Society of Japan*, 70, 22.
- Laha, S., Guainazzi, M., Dewangan, G. C., Chakravorty, S., & Kembhavi, A. K. 2014, *Monthly Notices of the Royal Astronomical Society*, 441(3), 2613–2643.
- McKernan, B., Yaqoob, T., & Reynolds, C. S. 2007, *Monthly Notices of the Royal Astronomical Society*, 379(4), 1359–1372.
- Midooka, T., Ebisawa, K., Mizumoto, M., & Sugawara, Y. 2022, *Monthly Notices of the Royal Astronomical Society*, stac1206.
- Mizumoto, M., Ebisawa, K., Tsujimoto, M., Done, C., Hagino, K., & Odaka, H. 2019, *Monthly Notices of the Royal Astronomical Society*, 482, 5316–5326.
- Nardini, E., Reeves, J. N., Gofford, J. et al. 2015, *Science*, 347(6224), 860–863.
- Parker, M. L., Pinto, C., Fabian, A. C. et al. 2017, *Nature*, 543(7643), 83–86.
- Pinto, C., Alston, W., Parker, M. L. et al. 2018, *Monthly Notices of the Royal Astronomical Society*, 476, 1021–1035.
- Strüder, L., Briel, U., Dennerl, K. et al. 2001, *Astronomy & Astrophysics*, 365(1), L18-L26.
- Takeuchi, S., Ohsuga, K., & Mineshige, S. 2013, *Publications of the Astronomical Society of Japan*, 65, 88.
- Tombesi, F., Cappi, M., Reeves, J. N., Palumbo, G. G. C., Yaqoob, T., Braito, V., & Dadina, M. 2010, *Astronomy and Astrophysics*,

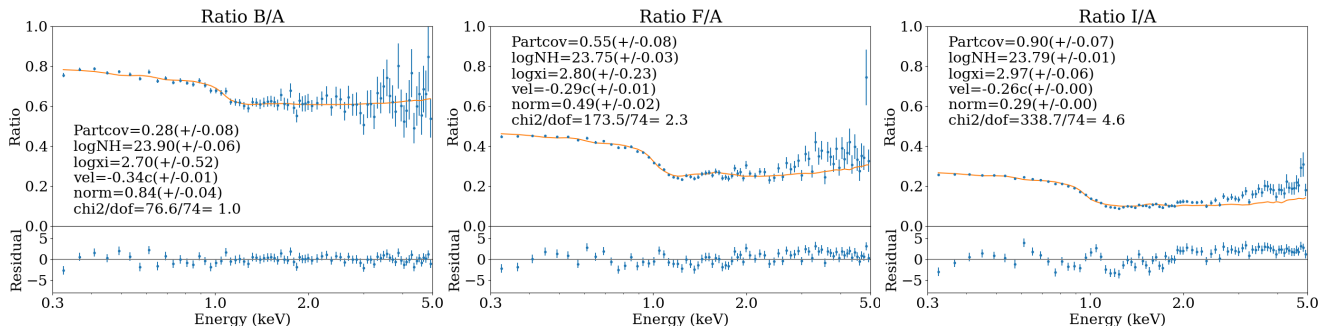


**FIGURE 5** Examples of the spectral-ratio model fitting (B/A, F/A, and I/A). Fitting of the dimmer ones shows more residuals above  $\sim 3$  keV, which may suggest changes in the PL index.

521, A57.